Development 128, 1493-1505 (2001)
Printed in Great Britain © The Company of Biologists Limited 2001
DEV3342

The *C. elegans* homolog of the murine cystic kidney disease gene *Tg737* functions in a ciliogenic pathway and is disrupted in *osm-5* mutant worms

Courtney J. Haycraft[1], Peter Swoboda[2], Patrick D. Taulman[1], James H. Thomas[2] and Bradley K. Yoder[1,*]

[1]Department of Cell Biology, University of Alabama at Birmingham Medical Center, Birmingham, AL 35294, USA
[2]Department of Genetics, University of Washington, Seattle, WA 98195, USA
*Author for correspondence (e-mail: byoder@uab.edu)

Accepted 8 February; published on WWW 5 April 2001

SUMMARY

Cilia and flagella are important organelles involved in diverse functions such as fluid and cell movement, sensory perception and embryonic patterning. They are devoid of protein synthesis, thus their formation and maintenance requires the movement of protein complexes from the cytoplasm into the cilium and flagellum axoneme by intraflagellar transport (IFT), a conserved process common to all ciliated or flagellated eukaryotic cells. We report that mutations in the *Caenorhabditis elegans* gene *Y41g9a.1* are responsible for the ciliary defects in *osm-5* mutant worms. This was confirmed by transgenic rescue of *osm-5(p813)* mutants using the wild-type *Y41g9a.1* gene. *osm-5* encodes a tetratricopeptide repeat (TPR)-containing protein that is the homolog of murine polaris (*Tg737*), a protein associated with cystic kidney disease and left-right axis patterning defects in the mouse. *osm-5* is expressed in ciliated sensory neurons in *C. elegans* and its expression is regulated by DAF-19, an RFX-type transcription factor that governs the expression of other genes involved in cilia formation in the worm. Similar to murine polaris, the OSM-5 protein was found to concentrate at the cilium base and within the cilium axoneme as shown by an OSM-5::GFP translational fusion and immunofluorescence. Furthermore, time-lapse imaging of OSM-5::GFP fusion protein shows fluorescent particle migration within the cilia. Overall, the data support a crucial role for *osm-5* in a conserved ciliogenic pathway, most likely as a component of the IFT process.

Movies available on-line:
http://www.biologists.com/Development/movies/dev3342.html

Key words: Cilia, Polaris, *Tg737*, *Y41G9a.1*, *osm-5*, Cystic kidney disease, *daf-19*, Tetratricopeptide repeat (TPR), Intraflagellar transport, *C. elegans*

INTRODUCTION

Cilia and flagella are present on many eukaryotic cells where they perform a variety of functions. Unicellular organisms such as *Trypanosoma brucei* and *Chlamydomonas* as well as sperm of many organisms use flagella for motility. Cilia function for fluid movement in the lung and are critical for normal function of the tissue. Motile cilia have also been implicated in embryonic patterning (Marszalek et al., 1999; Nonaka et al., 1998). In the mouse, loss of cilia caused by mutations in kinesins (Kif3a and Kif3b) leads to random left-right axis determination. According to the current model, beating of cilia on the node, a gastrulation stage organizing center, creates a leftward extra-embryonic fluid flow required for asymmetric distribution of a morphogen (Nonaka et al., 1998; Okada et al., 1999). In addition to motile cilia and flagella, there are numerous examples of immotile cilia that function in sensory perception such as chemoreception, photoreception and mechanoreception (Bargmann and Horvitz, 1991; Dwyer et al., 1998).

Cilia and flagella are complex organelles with more than 200 peptides involved in their formation, maintenance and function (Dutcher, 1995). Studies in *Chlamydomonas* have revealed a mechanism responsible for flagellar assembly termed intraflagellar transport (IFT) and an identical mechanism has been proposed for cilia (Cole et al., 1998; Piperno and Mead, 1997; Signor et al., 1999a). Through the generation of mutants, several of the key IFT peptides are being identified (Cole et al., 1998). As protein synthesis does not occur in the cilium, proteins required for axoneme assembly concentrate at the cilium base in rafts that are transported from the basal bodies towards the distal end of the cilium (anterograde movement) by kinesins and in the reverse direction (retrograde movement) by a dynein (Signor et al., 1999a). Thus, the basal body region appears to be a holding zone for IFT particles and their motor proteins.

While cilia are found on a broad spectrum of cells in mammals, in *C. elegans* they are only present in the nervous system on 60 of the 302 neurons of the adult hermaphrodite (Ward et al., 1975; Ware et al., 1975; White et al., 1986). Cilia extend from the dendritic tips of these neurons where they function as sensory organelles. Several mutations in *C. elegans* have been identified that specifically disrupt cilia formation on all or a subset of these sensory neurons (Culotti and Russell, 1978; Dusenbery et al., 1975; Starich et al., 1995). Mutations that affect the structure of all cilia, including *che-2*, *che-3*, *osm-*

1, *osm-5* and *osm-6*, result in defective osmotic avoidance (Osm), chemotaxis (Che) and dauer formation (Daf-d), as well as defective fluorescent dye uptake (Dyf), poor male mating behavior, and in many cases an extension of life span (Apfeld and Kenyon, 1999). Mutations in *osm-3* result in similar ciliary defects, but only in a subset of sensory neurons (Perkins et al., 1986).

Characterization of the molecular defects in these mutants with altered cilia structure has revealed that many of the proteins are homologs of IFT proteins identified in *Chlamydomonas* (Cole et al., 1998). The protein products of the worm *osm-1* and *osm-6* genes are homologs of IFT raft proteins identified in *Chlamydomonas*, while *che-3* and *osm-3* encode the dynein heavy chain DHC1b and a component of dimeric kinesin motor protein, respectively (Shakir et al., 1993; Signor et al., 1999a; Signor et al., 1999b). These genes are expressed in ciliated sensory neurons and their corresponding proteins localize to the distal end of the dendrites and within cilia. Furthermore, elegant studies by Scholey's laboratory using GFP translational fusion proteins demonstrated that OSM-1, OSM-3 and OSM-6 migrate in the cilia axoneme indicative of the IFT process (Orozco et al., 1999; Signor et al., 1999a). Further elucidation of the ciliogenic pathway in *C. elegans*, as well as other ciliated and flagellated eukaryotes awaits the characterization of additional proteins involved in the IFT process.

Accordingly, we have recently described the phenotype of a mutant mouse (*Tg737*$^{\Delta 2\text{-}3\beta Gal}$) where the function of a gene referred to as *Tg737* was abolished (Murcia et al., 2000). The protein encoded by *Tg737*, called polaris, contains ten copies of the tetratricopeptide repeat (TPR), a motif that mediates protein-protein interactions, often as part of large complexes (Blatch and Lassle, 1999; Moyer et al., 1994). Homozygous *Tg737*$^{\Delta 2\text{-}3\beta Gal}$ mutants die during midgestation, exhibit random left-right axis determination, and lack cilia on the ventral surface of the embryonic node. This phenotype is remarkably similar to that of the *kif3a* and *kif3b* kinesin mutants, both of which encode microtubule-based motor proteins implicated in IFT (Marszalek et al., 1999; Nonaka et al., 1998). Ciliary defects are also associated with the pathology in a hypomorphic allele of *Tg737* in the *Oak Ridge Polycystic Kidney* (*Tg737*^{orpk}) mutant mouse (Pazour et al., 2000; Taulman et al., 2001). These mice develop a complex pathology consisting of cystic kidneys, biliary and bile ductule hyperplasia, acinar atrophy in the pancreas, skeletal patterning defects and hydrocephalus (Moyer et al., 1994; Yoder et al., 1997; Taulman et al., 2001). The pathologies in the brain and the cystic renal lesions are associated with aberrantly formed cilia on the ependymal and the collecting duct cells, respectively. In agreement with these ciliary defects, polaris concentrates near the basal bodies at the apical surface of epithelia and in the cilia axoneme (Pazour et al., 2000; Taulman et al., 2001). Together these data suggest that polaris functions in a ciliogenic pathway and that it may be a component of the IFT system.

We further our analysis of *Tg737* function by characterizing its homolog in *C. elegans*, the gene *Y41g9a.1*. Our data indicate that mutations in *Y41g9a.1* are responsible for the ciliary defects seen in *osm-5* mutant worms. This is shown by the molecular characterization of three independent *osm-5* alleles and by rescue of the *osm-5* ciliary defects using the wild-type *Y41g9a.1* gene. Similar to what we have determined for *Tg737* and its corresponding protein polaris in the mouse, *osm-5* expression is consistent with this ciliogenic role. *osm-5* expression, as revealed by a GFP transcriptional fusion with the endogenous *osm-5* promoter, is detected in ciliated sensory neurons. In addition, the OSM-5 protein was found to concentrate at the distal end of the dendrites and within the cilia of the sensory neurons, as determined by immunofluorescence and in transgenic worms expressing an OSM-5::GFP translational fusion. Similar to other genes involved in the ciliogenic pathway in the worm, expression of *osm-5* is regulated by the RFX-type transcription factor DAF-19 (Swoboda et al., 2000). In addition, using the OSM-5::GFP translational fusion we demonstrate that OSM-5 migrates within cilia, as has been reported for OSM-1 and OSM-6 (Orozco et al., 1999; Signor et al., 1999a). Overall, the data substantiate a ciliogenic role for polaris and OSM-5 as components of the IFT system. Finally, owing to the high sequence conservation between *osm-5* and *Tg737*, the characterization of *osm-5* in the worm will probably yield a better understanding of *Tg737* function and how its disruption and subsequent ciliary defects lead to the complex pathology seen in the mouse.

MATERIALS AND METHODS

Strains and culture methods

Growth and culture of *C. elegans* strains were carried out as described (Brenner, 1974). All strains were grown at 20ºC, unless otherwise stated. Strains used for this study were: wild type N2 Bristol (Brenner, 1974), PR808 *osm-1(p808)*, PR811 *osm-6(p811)*, CB1033 *che-2(e1033)*, CB1124 *che-3(e1124)*, JT204 *daf-12(sa204)*, JT6924 *daf-12(sa204); daf-19(m86)*, DR86 *daf-19(m86)*, PR813 *osm-5(p813)*, SP1412 *osm-5(mn397)*, JT6150 *daf-11(m87); osm-5(sa130)*, and JT8651 *daf-19(m86)*/mnC1; *lin-15(n765)*. The following extrachromosomal arrays were used: adEx1262 (*gcy-5::gfp)* and adEx1268 *(gcy-8::gfp)* were employed as cell specific markers (Yu et al., 1997); saEx580-583 were used for X-box- and DAF-19-dependent *osm-5::gfp* expression analyses; saEx584-586 were assayed for *osm-5* transgenic rescue; yhEx19 and yhEx20 were used for in vivo IFT transport assays. All *osm-5* alleles used in this study have been previously described: *osm-5(p813)* (Culotti and Russell, 1978; Perkins et al., 1986); *osm-5(mn397)* (Starich et al., 1995); *osm-5(sa130)* (Starich et al., 1995; Vowels and Thomas, 1992).

Injection constructs, germline transformation and GFP expression analyses

The GFP transcriptional expression plasmid pCJ3 was constructed by inserting a 350 bp N2 genomic fragment containing approximately 300 bp of upstream sequence relative to the ATG and the first 16 codons of *osm-5* into the GFP expression vector pPD95.75 (gift from A. Fire). The PCR rescue fragment was amplified from N2 genomic DNA using AccuTaq polymerase (Sigma, St Louis, MO) and primers flanking the *osm-5* promoter and consensus polyA site (AATAAA). To generate the OSM-5::GFP translational fusion, the entire *osm-5* gene, including the 300 bp upstream promoter sequence, was amplified by long-range PCR of genomic DNA using AccuTaq polymerase. The PCR product was then cloned into the *Sal*I/*Xba*I site of pPD95.75. To ensure the correct translational reading frame, the junction between the vector and amplified PCR product was verified by sequencing.

N2 or *osm-5(p813)* adult hermaphrodites were transformed using standard techniques (Mello et al., 1991). Test DNA was injected at 5-

100 ng/μl along with pRF4, which contains the *rol-6(su1006)* dominant marker (Mello et al., 1991). Worms carrying the injected DNAs as stable extrachromosomal arrays were identified and maintained by their roller (Rol) phenotype. Rescue of *osm-5(p813)* cilia defects was assayed by analysis of amphid and phasmid neuron fluorescent dye filling, using DiI-C12 (Molecular Probes, Inc., Eugene, OR) as described (Fujiwara et al., 1999).

The X-box within the *osm-5* promoter region (GTTGCC AT AGTAAC) contained on the pCJ3 expression construct was mutated by overlapping PCR primed mutagenesis replacing the X-box with nonspecific nucleotides containing indicative restriction enzyme sites (*Mlu*I and *Ngo*MIV; ACGCGTGCCGGCTG). As verified by sequencing, plasmid junctions and the promoter fusion to *gfp* were correct and the entire promoter region contained in the pCJ3 construct was identical to wild type, except for the intended sequence changes. The promoter::GFP fusions were introduced into worms by germline transformation typically at 100 ng/μl. The injected strain JT8651 *daf-19(m86)*/mnC1; *lin-15(n765)* served as wild-type background, as *daf-19(m86)* is fully recessive. Segregating dauers were recovered at 15°C to obtain a *daf-19* homozygous background. GFP expression was analyzed in stable extrachromosomal transgenic lines at 1000× magnification (Zeiss Axioskop) by conventional fluorescence microscopy. Representative cohorts of animals of each genotype and transgenic line were examined at most developmental stages between the embryo and adult stage. Quantitative data (see Table 2) were obtained at the highest magnification on a standard stereo dissecting microscope (Wild Mikroskope) with a fluorescent light attachment (Kramer Scientific) only for the adult stage, as the transformation marker *lin-15* permits unambiguous detection of transgenics only at this stage. Examinations were performed blind, except when *daf-19* mutants were looked at, because the presence of dauers on the plates made blind scoring impossible. For comparisons, the relevant genotypes and X-box construct transgenes were analyzed side by side.

Neuronal cell anatomies and identities followed published descriptions (Hall and Russell, 1991; Ward et al., 1975; Ware et al., 1975; White et al., 1986).

For precise imaging of GFP expression in subcellular compartments and for in vivo intraflagellar transport (IFT) assays, a Deltavision microscopy setup (Silicon Graphics) was used. Worms at various developmental stages were put into 0.5 μl M9 buffer on a thin 2% agarose pad containing sodium azide as an anesthetic. For IFT assays, adult worms transgenic for the OSM-5::GFP translational fusion construct were anesthetized with 10 mM levamisole. Completely paralyzed worms were then observed with an inverted microscope (Zeiss Axiovert) at either a 63× or 100× (IFT assays) objective magnification (both objectives NA=1.40). This setup was equipped with a multiwavelength CCD camera (Quantix) and all shutters, filters and the stage were computer driven (Applied Precision). 3D data stacks were acquired in the FITC channel by moving the focal plane in 0.5 μm increments through the entire worm. For IFT assays, time-lapse fluorescent images were collected in only one focal plane at 1 frame per 0.5-0.6 seconds, and images were typically collected for 30 seconds total. Background and out-of-focus signals were removed using a conservative reiterative (15×) deconvolution algorithm (Agard et al., 1989; Scalettar et al., 1996). 3D data stacks were combined using maximum intensity projections of all data points along the *z*-axis. For IFT assays, movies were created from stacked images along the time axis using Deltavision and Adobe Premiere software. Still images were then taken from individual frames of time-lapse collections.

Molecular biology

Standard molecular biology techniques were used (Sambrook et al., 1989). The original *osm-5* cDNA was isolated from a mixed stage *C. elegans* Uni-ZAP XR cDNA library (Stratagene, La Jolla, CA) and by RT-PCR from total worm RNA. Reverse transcription reactions were carried out using 10 μg total RNA from mixed stage worms and Moloney Murine Leukemia Virus-Reverse Transcriptase (MMLV-RT) (Promega, Madison, WI) according to the manufacturer's instructions. PCR was performed with Taq polymerase (Eppendorf Scientific, Inc., Westbury, NY). Sequencing of all cDNAs and the initial pCJ3 injection construct was performed by the UAB Sequencing Facilities using ABI Prism model 377. BLAST searches to identify *D. melanogaster* and *X. laevis* homologs were performed using the National Center for Biotechnology Information BLAST service (http://www.ncbi.mln.nih.gov/blast/blast.cgi). The *T. brucei* homolog was identified using the Sanger Center BLAST server (http://www.sanger.ac.uk/cgi-bin/nph-Blast_Server.html). All *C. elegans* genome sequence information used for this study was obtained directly from the *C. elegans* Genome Sequencing Centers (http://www.sanger.ac.uk/Projects/C_elegans/ and http://genome.wustl.edu/gsc/C_elegans) (*C. elegans* Sequencing Consortium, 1998). The X-box was identified by visual inspection of the *osm-5* promoter region.

Northern blot analysis

Worms for RNA isolation were lysed by addition of five volumes of 4M guanidine isothiocyanate and homogenization using a PowerGen 700 (Fisher Scientific, Pittsburgh, PA). Particulate matter was removed by centrifugation at 6000 ***g*** and RNA was purified by centrifugation over a CsCl cushion. PolyA-enriched RNA was isolated using an Oligotex mRNA kit (Qiagen, Valencia, CA). Radiolabeled antisense *osm-5* and *act-123* (Krause et al., 1989) probes were synthesized using the Riboprobe Synthesis kit (Promega, Madison, WI). For *daf-19* expression analysis, both control and experimental strains contained the *daf-12(sa204)* mutation to suppress the Daf-c phenotype of *daf-19(m86)*.

Antibody production

A cDNA fragment corresponding to amino acids 238 through 660 of OSM-5 protein was cloned into pGEX-5x-1 (Clontech Laboratories, Palo Alto, CA). Recombinant fusion protein was purified over GST sepharose columns as previously described (Frangioni and Neel, 1993). BALB/C mice were immunized with 100 μg of OSM-5::GST fusion protein in complete Freund's adjuvant injected subcutaneously into the hind legs. Subsequent boosts, given on days 3, 10, 15 and 20, consisted of 50 μg of antigen in phosphate buffered saline (PBS) administered in a similar manner. On day 21, cells from popliteal and inguinal lymph nodes were collected and fused with the P3X63-Ag8.653 myeloma line according to standard procedures. Fused cells were suspended in HAT media and seeded into 24-well tissue culture plates. Fourteen days after fusion, supernatants were screened for anti OSM-5 antibodies by ELISA. The ability of the antibodies to recognize an epitope contained on OSM-5 was evaluated by Western blot analysis of OSM-5::GST and GST proteins purified from *E. coli* using a 1:5000 dilution of 4A1 or 12B6 ascites.

Immunofluorescence

Whole-mount fixation and permeabilization of mixed stage larvae and adult worms were carried out as described (Miller and Shakes, 1995). Fixed and permeabilized worms were incubated with a 1:400 dilution of ascites (4A1 or 12B6), or no primary antibody as a negative control, overnight at 4ºC in AbA (1% bovine serum albumin (BSA); 0.5% Triton X-100; 1× phosphate buffered saline). Following incubation, worms were washed with multiple changes of AbB (0.1% bovine serum albumin; 0.5% Triton X-100; 1× PBS) over a 3 hour period. Worms were then incubated with a 1:400 dilution of Texas Red-conjugated goat-anti mouse secondary antibody (Molecular Probes, Eugene, OR) in AbA for 2 hours at room temperature. Worms were washed extensively as described above and nuclei were stained using Hoechst No. 33528 (Sigma) diluted 1:1000 in wash buffer. Samples were mounted on slides with mounting media (90% glycerol with 10 mg/ml p-phenylene diamine). No specific staining was detected in any secondary antibody only control. For blocking studies, antibodies

were preincubated with a 10-fold molar excess of purified OSM-5::GST or GST protein. The GST proteins were then removed by incubation with two rounds of GST affinity resin and the resulting depleted antisera used in the immunofluorescence analysis as above.

For polaris localization in the mouse, tissue samples were isolated from wild-type animals, embedded in OCT, cut into 5 μm sections and fixed for 10 minutes with 4% formaldehyde, 0.2% Triton-X 100 in PBS. Sections were incubated in blocking buffer (1% BSA in PBS) for 10 minutes, followed by a 45 minute incubation with affinity-purified polyclonal anti-polaris antibody and commercial monoclonal anti-β-tubulin IV antibody (Biogenex, San Ramon, CA) diluted in blocking buffer. After three washes in PBS, slides were incubated for 45 minutes in TRITC-conjugated goat anti-rabbit and FITC-conjugated goat anti-mouse secondary antibodies (Jackson ImmunoResearch Laboratories, West Grove, PA) diluted in blocking buffer and mounted as described above. Specificity of the anti-polaris antibody was confirmed by Western blot analysis of protein extracts isolated from $Tg737^{\Delta 2\text{-}3\beta Gal}$-null mutant and wild-type mice (Murcia et al., 2000; Taulman et al., 2001).

RESULTS

Cloning and structural analysis of *Y41g9a.1*

The *Tg737* gene was first identified in the mouse through an insertional mutation that caused polycystic kidney disease and skeletal patterning defects (Moyer et al., 1994). Polaris, the protein encoded by *Tg737*, contains ten copies of a degenerate motif called the tetratricopeptide repeat (TPR) thought to mediate protein-protein interactions. While the function of polaris is not known, the localization of the protein to basal bodies and cilia axonemes along with the loss of cilia in mice mutant for *Tg737* suggest that it is involved in ciliogenesis (Murcia et al., 2000; Pazour et al., 2000; Taulman et al., 2001). To facilitate further analysis of polaris function, we searched the genome databases using BLASTX to identify a potential homolog in *C. elegans*. The only significant homology was found in the gene *Y41g9a.1*, which is located on the left arm of linkage group X. Using oligonucleotide primers corresponding to the *Y41g9a.1* gene, we isolated the *Tg737* homolog from a mixed stage cDNA library and independently by reverse transcriptase-PCR (RT-PCR). Comparing the cDNA and genomic sequences indicates that *Y41g9a.1* has 15 exons spanning over 7 kb of genomic sequence. Conceptual translation of the 2.5 kb open reading frame predicts an 820 amino acid protein. The predicted amino acid sequence of Y41G9A.1 protein shares 45% identity and 62% homology with murine polaris (Fig. 1). Like the mouse protein, Y41G9A.1 is predicted to contain ten TPR repeats, three tandem repeats toward the N terminus and seven tandem repeats near the C terminus of the protein. Additional BLASTX searches indicate that polaris sequence is also highly conserved in other organisms including *Homo sapiens* (Schrick et al., 1995), *Gallus gallus*, *Xenopus laevis*, *Drosophila melanogaster* and *T. brucei* (Fig. 1). A high degree of homology is present not just in the TPRs but also across much of the protein, suggesting that polaris may function in a similar pathway in all these organisms.

Mutations in the *Y41g9a.1* gene are responsible for the ciliary defects in *osm-5* mutant worms

Many mutations have been identified in *C. elegans* that disrupt cilia formation (Perkins et al., 1986; Starich et al., 1995). While several of the genes responsible for cilia morphology have been identified, the underlying genetic cause responsible for cilia defects in *osm-5* mutants remained elusive. *osm-5* mutants were originally isolated in an ethyl methanesulfonate (EMS) mutagenesis screen to identify genes required for normal osmotic avoidance behavior (Culotti and Russell, 1978). In addition to defects in osmotic avoidance, electron microscope analysis of *osm-5(p813)* mutant worms revealed morphological defects in ciliated endings of all sensory neurons (Perkins et al., 1986). We confirmed and extended these data by using GFP fusions that are expressed in specific sensory neurons throughout development (Fig. 2 and Table 1; Yu et al., 1997). ASE is a chemosensory neuron in the head with a cilium exposed to the external environment (Fig. 2A-C; Bargmann and Horvitz, 1991). We found that *osm*-5 mutants specifically lack the distal parts of cilia (Fig. 2E). Cilia from wild-type animals were clearly distinguishable from those in *osm*-5 mutants (compare Fig. 2D with 2E). As a control, we examined a GFP fusion that is expressed specifically in AFD, a thermosensory neuron in the head (Mori and Ohshima, 1997) with a rudimentary cilium and many finger-like projections (microvilli) (Fig. 2A,B,F). The finger-like microvilli at the distal end of the AFD dendrite were not visibly affected in *osm*-5 mutants (compare Fig. 2G with 2H). Subcellular compartments other than the cilia in both of these neurons were essentially unaffected in *osm*-5 mutants, demonstrating that the morphological defects in *osm-5* mutants are cilium specific (Table 1). As was reported for several other cilia structure mutants (Peckol et al., 1999), we occasionally found short extraneous processes emanating from or near the cell body in *osm*-5 mutants (Table 1). The abnormalities in cilia structure of *osm-5* mutants lead to defective osmotic avoidance (Osm), chemotaxis (Che), dauer formation (Daf-d), fluorescent dye uptake by specific amphid and phasmid neurons (Dyf), male mating ability and an increase in the normal life span (Apfeld and Kenyon, 1999).

Genetic mapping studies place *osm-5* on the left arm of linkage group X near the location of the *Y41g9a.1* gene. As both *Tg737* mutant mice and *osm-5* mutant worms are

Table 1. Morphology of two sensory neuron classes

ASE (visualized with *gcy-5*::gfp)*

Genotype	Cilium	Dendrite	Cell body, axon	Additional process‡
Wild type	93 (full length) 7 (shortened)	100	100	2
osm-5	3 (full length) 97 (shortened)	100	100	8

AFD (visualized with *gcy-8*::gfp)*

Genotype	Microvilli	Dendrite	Cell body, axon	Additional process‡
Wild type	100	100	100	2
osm-5	100	100	100	5

*Data are percentages: the presence and morphological appearance of different subcellular compartments were observed by conventional fluorescence microscopy. Animals at the L1 or L2 larval stage were analyzed, as the two sensory neurons ASE and AFD are born during embryogenesis. Between 55 and 65 animals were analyzed for each genotype. Wild type, N2 Bristol; *osm-5*, *osm-5 (p813)*.

‡Additional process describes mostly short extraneous processes emanating either from the cell body or from axon bifurcations.

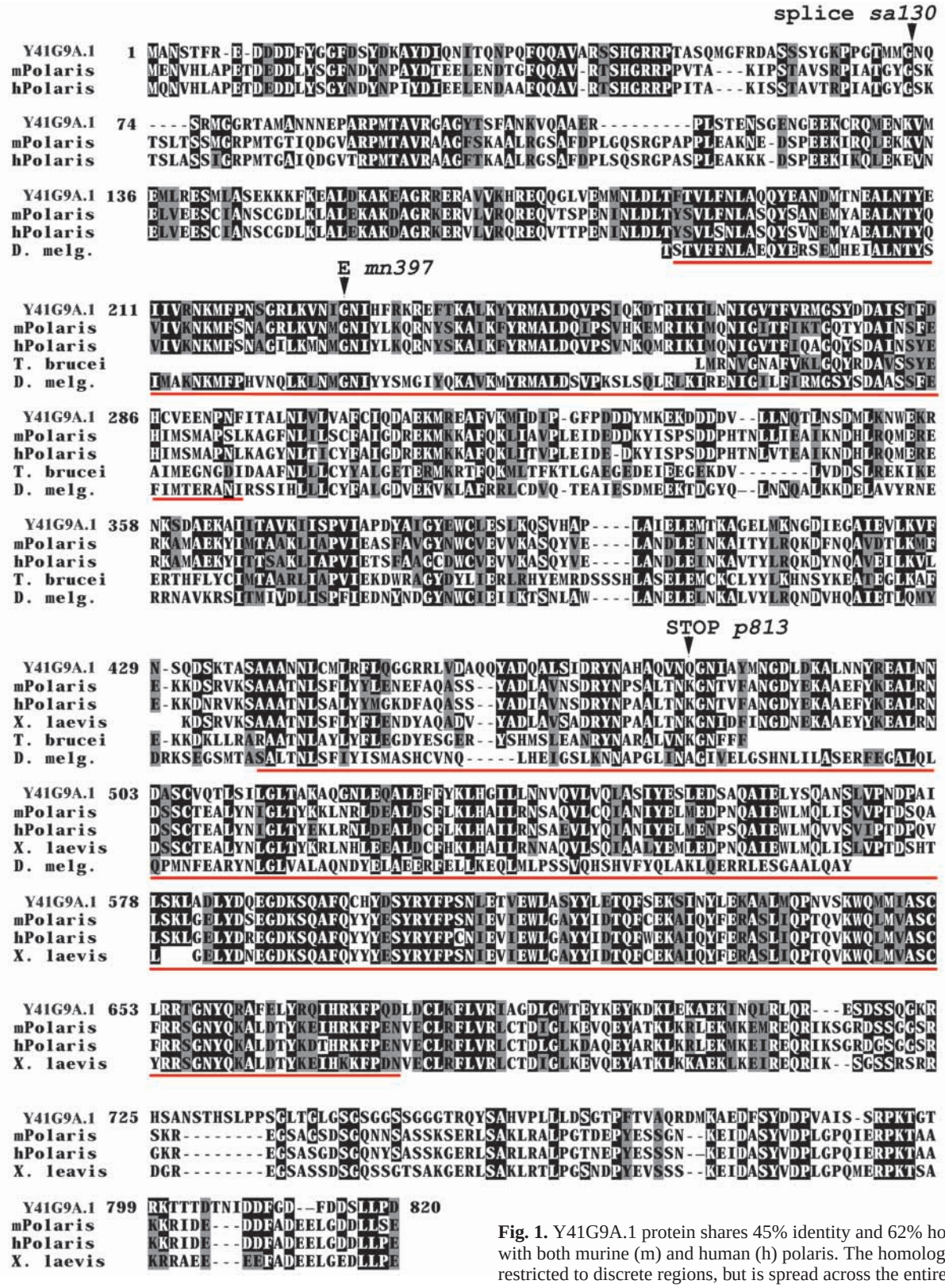

Fig. 1. Y41G9A.1 protein shares 45% identity and 62% homology with both murine (m) and human (h) polaris. The homology is not restricted to discrete regions, but is spread across the entire length of the protein. BLAST searches identified partial sequences of homologs in *Drosophila melanogaster* (predicted gene CG12548), *T. brucei* (sheared genomic clones 53F4.TF, 17A15.TF and 107C12.TF) and *X. laevis* (ESTs cm39h06.w1, b108a08.w1, bl11c05.w1 and cm61b06.w1). Highlighted regions indicate similarity (gray) and identity (black). The TPR motifs predicted in mouse and human polaris and Y41G9A.1 protein are underlined in red. The locations of the mutations identified in the three *osm-5* alleles described in the text are indicated with arrowheads.

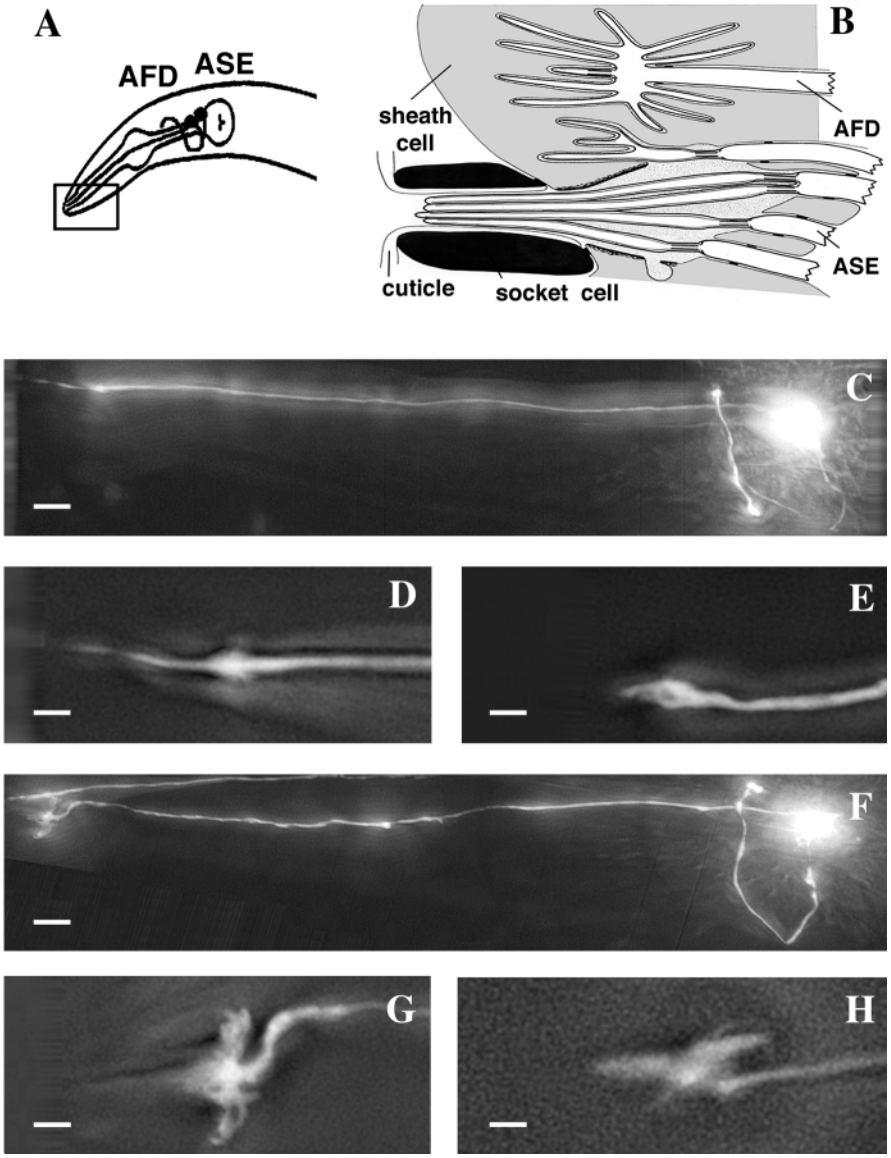

Fig. 2. Cilia defects of sensory neurons in *osm-5* mutants. Transgenic animals harboring ciliated sensory neuron specific GFP markers (*gcy-5::gfp* and *gcy-8::gfp*; Yu et al., 1997; compare with Table 2) were used to visualize cilia in wild type and in the cilium structure defective mutant *osm-5*. Anterior is towards the left and dorsal is upwards. (A) The positions in the head of bipolar ciliated sensory neurons ASE and AFD. For the bilateral pairs ASE and AFD of the amphid sensilla, only the left neurons are shown. Cell bodies are dots. The axons of AFD and ASE enter the nerve-ring between the two pharyngeal bulbs, the dendrites extend anteriorly to the tip of the nose. The sensory endings of both neurons are positioned at the tip of the dendrites and are not distinguishable in this drawing. The rectangle depicts the areas shown in B,D,E,G,H). (B) The sensory endings of some amphid sensory neurons (from Perkins et al., 1986). Dendritic tips are shown towards the right. Sensory endings extend from these dendritic tips. The cilium of ASE is exposed to the environment. The microvilli of AFD are encased within the amphid sheath cell. (C) GFP expression (*gcy-5::gfp*) in ASE at the L1 larval stage, illuminating the entire cell (GFP marker expression only in ASER). (D,E) The sensory ending (cilium) of ASE in L1 larvae. The cilium is visible as a thin projection at the tip of the dendrite (thick process to the right). The cilium is full length in wild type (D) and severely reduced in length in the *osm-5* mutant (E). Similar phenotypes were observed throughout development. (F) GFP expression (*gcy-8::gfp*) in AFD at the L1 larval stage, illuminating the entire cell (foreground: AFDL, partially visible in the background: AFDR). (G,H) The sensory endings (microvilli) of AFD in L1 larvae. Microvilli are clearly visible as finger-like projections at the tip of the dendrite (thick process to the right). AFD has only a rudimentary cilium, which is not visible here. Microvilli were indistinguishable between wild-type (G) and *osm-5* mutant (H) backgrounds throughout development. Scale bars: 5 μm in C,F; 2 μm in D,E,G,H.

associated with ciliary defects, we predicted that the *Y41g9a.1* gene was responsible for the *osm-5* ciliary pathology. To begin evaluating this possibility, we sequenced *Y41g9a.1* cDNA from three independent *osm-5* alleles. In each case, a point mutation in the *Y41g9a.1* cDNA was detected and subsequently confirmed in the corresponding region of the genomic DNA, which established the gene *Y41g9a.1* as *osm-5*. In *osm-5(p813)*, a C to T transition at position 1435 of *osm-5* cDNA results in a stop codon at amino acid 473. The predicted OSM-5 protein would contain the complete N-terminal set of three TPRs but would lack the C-terminal half of the protein including six of the seven TPR motifs (Fig. 1). In the *mn397* allele, a missense mutation at amino acid 229 results in a glycine to glutamate substitution (Fig. 1). This glycine is located at position 8 in the second TPR motif and is an invariant residue present in all *Tg737* protein homologs analyzed to date. Furthermore, it is a crucial residue identified in other TPR-containing proteins where it is most often a glycine or small hydrophobic residue such as alanine or serine (Das et al., 1998). In the final allele analyzed, *osm-5(sa130)* a point mutation was detected at the 5′ donor splice site (position 214) of exon three (Fig. 1). The cDNA clone sequenced from *sa130* contained a four-nucleotide insertion that resulted in a frame shift.

To confirm that the mutations identified above were directly responsible for the cilia defects in *osm-5* mutants, a 7.6 kb fragment consisting of 240 base pairs upstream of the coding sequence, the exon regions, introns and consensus poly-A signal (AATAAA) was amplified from wild-type genomic worm DNA. *Y41g9a.1* is the only open reading frame predicted within this genomic sequence. This PCR fragment was introduced into *osm-5(p813)* mutant worms by germline transformation. Stable transgenic lines were assayed for fluorescent dye filling of amphid and phasmid neurons using

DiI-C12 (data not shown). Introduction of the wild-type *Y41g9a.1* gene into the *osm-5(p813)* mutant background was sufficient to restore cilia and allow dye uptake. In contrast, *osm-5* mutants uninjected or injected with the *rol-6(su1006)* marker DNA alone remained fluorescent dye-filling defective (data not shown). Together, the identification of three independent mutations in *Y41g9a.1* and the restoration of cilia in *osm-5* mutants by the expression of the wild-type *Y41g9a.1* gene confirm that *Y41g9a.1* is the same gene as *osm-5*.

osm-5 is expressed in ciliated sensory neurons

To examine the developmental expression pattern of *osm-5*, Northern blot and RT-PCR analyses were performed using RNA isolated from synchronized worms. A 2.6 kb transcript was observed at highest levels during embryogenesis and early larval stages using Northern blot analysis. Expression decreased, relative to actin controls, to almost undetectable levels during L4 and adult stages (Fig. 3A). RT-PCR analysis confirmed that *osm-5* is still expressed in both L4 and adult worms, albeit at very low levels (data not shown).

To determine which cells express *osm-5*, a transcriptional fusion was generated between GFP and the *osm-5* promoter. The promoter fragment consisted of 240 base pairs upstream of the *osm-5* gene and 16 codons of the first exon (pCJ3 construct). In agreement with Northern analysis, GFP expression in animals transgenic for pCJ3 was first observed around the twofold stage of embryogenesis and continued throughout development and in the adult worm. The pattern of GFP fluorescence was consistent with expression in all ciliated sensory neurons including the amphids, phasmids, and inner and outer labials (Fig. 3B,C). GFP expression was also observed in the sensory rays of the male tail (data not shown). Thus, similar to the expression of *Tg737* in the mouse, *osm-5* is strongly associated with ciliated cells. In addition, the pattern of *osm-5* expression is remarkably similar to that reported for other genes involved in ciliogenesis in the worm including *che-2*, *che-3*, *daf-19*, *osm-1* and *osm-6* (Collet et al., 1998; Fujiwara et al., 1999; Signor et al., 1999a; Swoboda et al., 2000; Wicks et al., 2000). The timing of *osm-5*::GFP appearance correlates well with the formation of cilia in *C. elegans*, which starts at the two-fold stage of embryogenesis (Fujiwara et al., 1999). Reporter constructs that carried additional upstream sequence (roughly 3.5 kb) showed a similar pattern and level of GFP expression as the 240 bp promoter (data not shown), indicating that the 240 bp promoter is sufficient for expression of *osm-5* in ciliated sensory neurons.

Localization of OSM-5 protein in wild-type worms

To evaluate the potential role for OSM-5 protein in a ciliogenic pathway and to determine its localization within *C. elegans* sensory neurons, we generated monoclonal antibodies against bacterially expressed recombinant OSM-5 protein (amino acids 238-660) fused to GST. Two different monoclonal antibodies were used in this study. Several experiments were conducted to evaluate their specificity. First, the ability of antibodies to recognize an epitope on the OSM-5 protein was evaluated on western blots that contained purified OSM-5::GST protein and a GST protein. Both monoclonal antibodies used in this study strongly recognize the OSM-5::GST protein but not the GST protein alone in the adjacent lane (Fig. 4). After Western analysis, it is clear that 4A1 and 12B6 recognize multiple smaller proteins. These smaller peptides are detectable upon Coomassie Blue staining and are only in the lane containing the fusion protein; thus, they probably represent degradation products of the OSM-5::GST protein that arise during purification from *Escherichia coli*. It is interesting that 12B6 appears to be more reactive with several of the lower molecular weight peptides than 4A1, suggesting that the antibodies may bind different epitopes within OSM-5.

As the above data suggests that the 12B6 and 4A1 recognize an epitope on OSM-5, we analyzed OSM-5 localization in wild-type N2 worms by immunofluorescence. Using either antibody, prominent OSM-5 protein staining was observed in

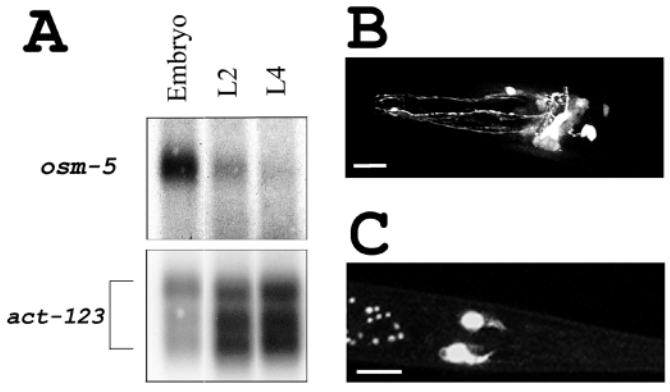

Fig. 3. Expression of *osm-5*. (A) Northern blot analysis of staged populations of worms. *osm-5* expression is first observed during embryogenesis and decreases throughout development relative to *act-123* controls. (B,C) Expression of *gfp* in adult worms driven by a 240 bp *osm-5* promoter is consistent with expression in ciliated sensory neurons. Anterior is towards left in both images. (B) In the head of the worm, GFP is easily detected in the process bundles that extend to the tip of the nose of the worm. (C) Dorsal view of the phasmid neurons. *osm-5* expression is shown in one pair of phasmid neurons. The second pair is out of the plane of focus. Scale bars: 10 μm.

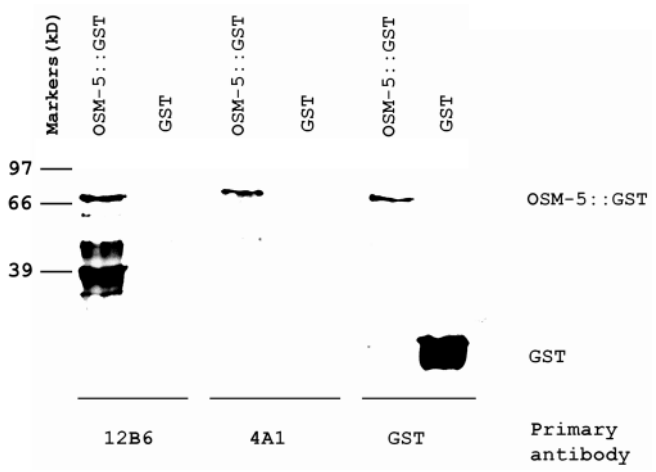

Fig. 4. Western blot analysis of monoclonal antibodies. Equal amounts of purified OSM-5::GST and GST were probed with ascites, 4A1 or 12B6 or anti-GST antibodies to show specificity of monoclonal antisera. GST antibodies recognize both recombinant OSM-5::GST and GST, whereas 12B6 and 4A1 recognize OSM-5::GST but not GST alone.

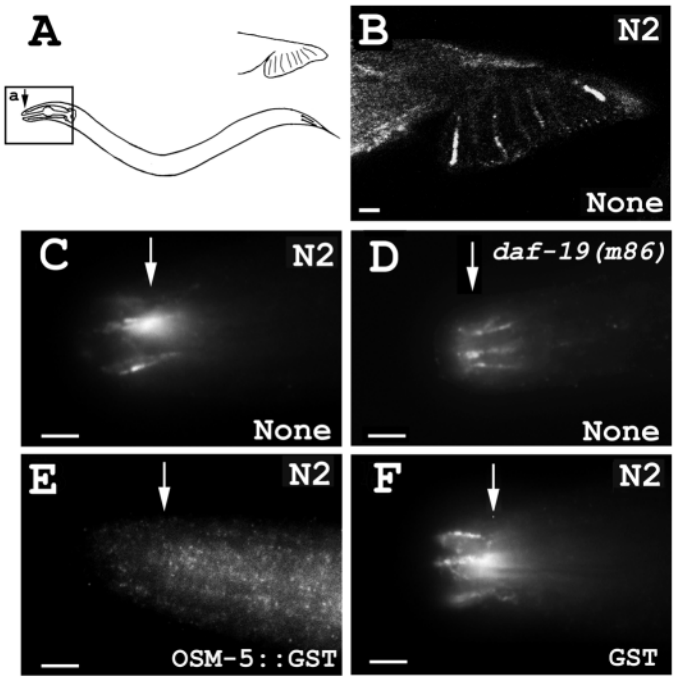

Fig. 5. Immunolocalization of OSM-5 protein and antibody specificity. All panels are lateral views of wild type (B,C,E,F) or *daf-19(m86)* (D) worms processed in parallel for immunofluorescence using the 12B6 antibody. Anterior is leftwards and dorsal is upwards. (A) A hermaphrodite worm (bottom) and a lateral view of the male tail (top). Box 'a' indicates the region pictured in C-F. Arrows indicate the position of the amphid cilia. In unblocked samples, immunoreactivity is observed in the rays of the male tail (B) and the ciliated amphid and labial neurons (C). Preincubation of the antibody with 10-fold molar excess of purified OSM-5::GST (E) blocks all immunostaining in the amphid and labial neurons, while preincubation of the antibody with purified GST alone (F) has no effect. (D) In the absence of DAF-19, low levels of OSM-5 protein are observed at the tips of dendrites despite the loss of cilia associated with mutations in *daf-19*. Scale bars: 5 μm.

the transition zones and cilia of the sensory neurons, including the amphids, phasmids, labials and rays of the male tail (Fig. 5B,C; data not shown). This localization is in agreement with *osm-5*::GFP expression and the ciliary defects in *osm-5* mutant worms. Little or no staining was observed in the cell bodies or other areas of the worm and no specific staining was evident with the pre-immune sera or the secondary antibody-only controls.

To evaluate the specificity of the antisera further, we preblocked the antibodies with 10-fold molar excess of either OSM-5::GST or GST proteins prior to immunolocalization. Preincubating the antisera with the OSM-5::GST fusion but not the GST protein alone abolished the immunolocalization in the sensory neurons of both the amphids and phasmids (Fig. 5C,E,F; data not shown). These data suggest that the immunolocalization patterns detected with these antibodies are due to the OSM-5 protein.

To evaluate the localization of the OSM-5 protein further, we generated several lines of transgenic worms that express an OSM-5::GFP translational fusion under the regulatory control of the 240 base pair fragment used to drive the GFP transcriptional fusion above. The OSM-5::GFP translational fusion construct was injected into *osm-5(p813)* mutants. All transgenic lines were screened for dye filling of the amphid and phasmid neurons to confirm rescue of the *osm-5(p813)* cilia defects and show that the OSM-5::GFP fusion protein was functional. Analysis of OSM-5::GFP expression reveals almost exclusive localization to the transition zones and cilia of amphids, phasmids, labials and rays of the male tail (data not shown). This result is identical to the immunolocalization of OSM-5 using the monoclonal antibodies. Furthermore, the localization of OSM-5 to the transition zones and cilia in *C. elegans* is consistent with the expression and subcellular localization of its mammalian counterpart, polaris. In the mouse, polaris is expressed predominantly in ciliated epithelia of the lung, brain, and efferent duct where it concentrates at the base of cilia and in the axoneme (Fig. 6; data not shown; Taulman et al., 2001).

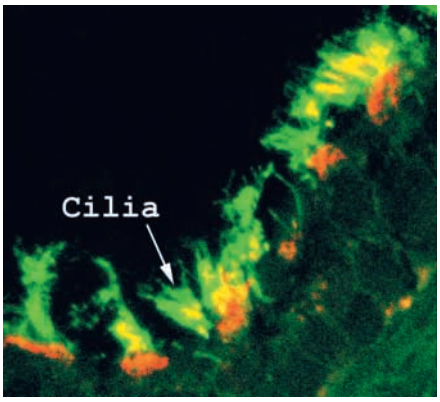

Fig. 6. Immunolocalization of polaris in the mouse. Mouse efferent duct was co-stained for polaris (red) and β-tubulin IV (green). Polaris can be observed in a structure at the base of the cilia (basal body) as well as in the cilia axoneme.

Localization of OSM-5 protein in worms with ciliary defects

As we identified several mutations in *osm-5* cDNAs, we wanted to determine if these mutations affect expression or localization of the OSM-5 protein. In each mutant line analyzed (*p813* (the reference allele), *sa130*, and *mn397*), OSM-5 expression was still detected at the transition zones by immunolocalization (data not shown). However, it should be noted that in the *sa130* allele there was a consistent reduction in the level of protein relative to the other mutants using either of the monoclonal antisera. Given that the splice site mutation in the *sa130* allele occurs upstream of the region in OSM-5 used to generate the antibodies, it was surprising that the OSM-5 protein was still detected in the truncated cilia by immunofluorescence. Thus, it is feasible that both of the OSM-5 monoclonal antibodies used in this study recognize an epitope contained on another ciliary protein. Although we were unable to directly demonstrate this, it is possible that there are alternatively spliced *osm-5* mRNAs or that the mutation in the *sa130* allele allows some residual product to be produced from an aberrant splice site as has been reported for similar mutations due to Tc1 insertions in the worm (Rushforth and Anderson, 1996).

In addition to the *osm-5* mutant worms, several other

mutations have been identified that disrupt formation of cilia in *C. elegans* (Perkins et al., 1986). We analyzed OSM-5 localization in a subset (*che-2(e1033)*, *che-3(e1124)*, *osm-1(p808)*, *osm-6(p811)*, and *daf-19(m86)*) of these mutations that result in similar ciliary defects as seen in *osm-5* worms. In all of these mutants, OSM-5 protein was still observed at the distal tips of the dendrites at the transition zones where cilia would form (data not shown). However, in the dynein mutant *che-3(e1124)*, the staining was generally more intense at the distal end of the dendritic tips. This possibly indicates that OSM-5 protein becomes concentrated in the electron dense material characteristically found at the distal tips of the truncated cilia in *che-3* mutants (Perkins et al., 1986). The same result has been reported for OSM-6, where it was attributed to the loss of retrograde IFT raft movement in the *che-3* mutants (Collet et al., 1998). Another interesting observation is that while OSM-5 protein is still found at the dendritic tips of *daf-19* mutants, the level of OSM-5 protein expression was markedly reduced relative to that seen in wild-type worms (Fig. 5C,D). This result suggests that DAF-19 might be important for normal *osm-5* expression as was reported for several other ciliogenic genes in the worm (Swoboda et al., 2000).

DAF-19 regulation of *osm-5* expression

DAF-19 is a transcription factor known to regulate the expression of several genes (i.e. *che-2*, *osm-1* and *osm-6*) that are required for proper cilia formation in *C. elegans* (Swoboda et al., 2000). DAF-19 is the only RFX-type transcription factor in *C. elegans* and mediates its transcriptional regulation through a conserved palindromic sequence referred to as the X-box, located approximately 100 nucleotides upstream of the translational start site (Swoboda et al., 2000). The fact that the X-box is found in the promoters of multiple ciliogenic genes that are expressed in a similar pattern as *osm-5*, along with the reduced levels of OSM-5 protein seen in the *daf-19* background, suggested that *osm-5* expression might be under DAF-19 control.

To begin evaluating the possible role of DAF-19 in the regulation of *osm-5*, we analyzed the 240 bp region upstream of the putative *osm-5* translational start site for a potential X-box sequence. To facilitate this analysis, we compared this 240 bp region with the corresponding upstream sequence of the *osm-5* homolog in the closely related nematode *C. briggsae* (located on cosmid G41B17), as promoter elements are typically more conserved than intergenic sequences. Interestingly, a near consensus DAF-19 binding site was identified in both species located at positions –115 in *C. elegans* and at –91 in *C. briggsae* (Fig. 7A). To explore the role of this putative X-box, we measured the relative expression levels using the pCJ3 GFP-fusion construct in wild type and *daf-19* mutants. As seen previously, the 240 base pair promoter drove moderate levels of GFP expression in ciliated sensory neurons (Table 2). Similar to what we found for the OSM-5 protein by immunofluorescence, moving this transgene into a *daf-19* mutant background resulted in a significant reduction in the levels of GFP in the two independent lines tested. To further evaluate the importance of the X-box in *osm-5* expression, we mutated the X-box in pCJ3 and measured GFP expression in wild-type worms. Disruption of the X-box resulted in much lower levels of GFP expression and in fewer

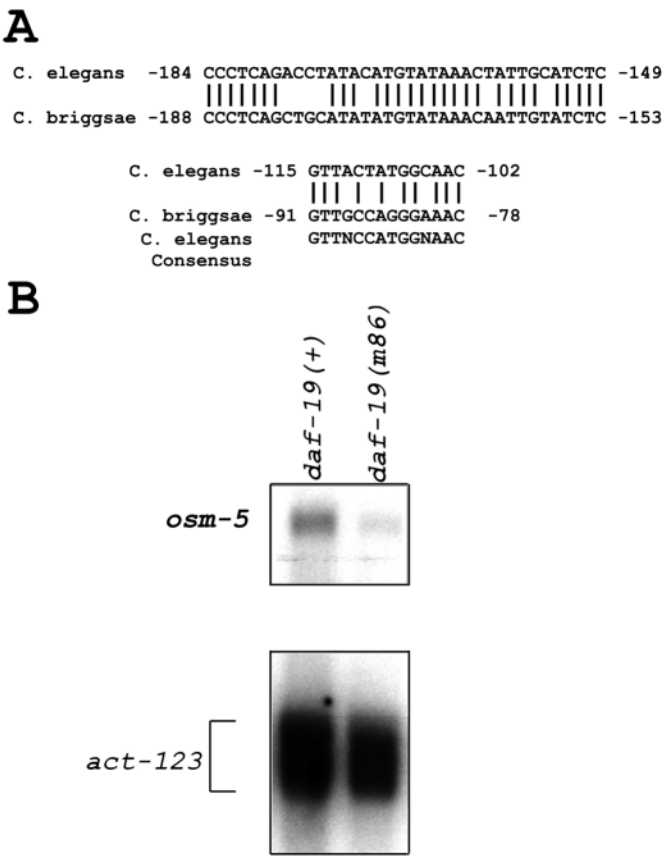

Fig. 7. *osm-5* expression is regulated by DAF-19. (A) Two potential promoter elements were identified based on their sequence similarity in *C. elegans* and *C. briggsae*, two closely related nematodes. The proximal element closely resembles the consensus X-box sequence that has been identified in the promoters of several cilia specific genes where it is required for DAF-19-dependent expression in ciliated sensory neurons. The distal element contains 75% identity between the two species. Although no factor has been identified that recognizes all or part of this element, its high conservation suggests it may be involved in regulating expression of *osm-5*. (B) Northern blot analysis of poly A-enriched RNA from *daf-19(+)* and *daf-19(m86)*, a putative null allele. In the absence of functional DAF-19, expression of *osm-5* is severely reduced, but not eliminated, relative to *act-123*.

Table 2. Expression analyses using an in vivo GFP expression assay*

Type of X-box	Wild type		Mutated
Genotype	Wild type	*daf-19*	Wild type
osm-5::gfp	94	4	49
	71	0	3
	54	nd	0
	13	nd	0
Strength of expression	Moderate	Weak/absent	Weak/absent

*Data are given as percent expression in ciliated sensory neurons in the head of adult animals. *osm-5::gfp* is expressed in most of the 60 ciliated sensory neurons of the animal. Four independent transgenic lines were analyzed. Each number represents the data for one transgenic line. For two transgenic lines containing the wild-type X-box sequence, the transgene was also moved from the wild-type into a *daf-19* background. Between 60 and 100 animals were analyzed for each transgenic line. nd, experiment not done.

cells (Table 2). Finally, the GFP expression and reduced OSM-5 protein staining in *daf-19* mutants was corroborated by Northern blot analysis, where the level of *osm-5* mRNA was dramatically reduced in the absence of DAF-19 function (Fig. 7B). Together, these data show that the X-box dramatically affects the level of *osm-5* expression in a DAF-19-dependent manner, as shown for several other cilia specific genes (Swoboda et al., 2000). Thus, DAF-19 may function as a key regulator of the ciliogenic pathway suggesting that searching the *C. elegans* genome for correctly spaced X-box sequences in promoters may be a productive means of identifying other components of the pathway.

It should be noted that in the *daf-19* background *osm-5* expression was not completely abolished. This result suggests that DAF-19 may not be the sole regulator of *osm-5*. Therefore, it is noteworthy that a second highly conserved sequence was identified in the promoter region in *C. elegans* and *C. briggsae*. This sequence element is located in similar positions in the promoters in *C. elegans* (at –184) and in *C. briggsae* (at –188). The sequence element is 36 nucleotides in length and shares nearly 75% identity between the two species (Fig. 7A). Although no potential binding factor has yet been identified, the high conservation with regards to sequence and spacing suggests that it may be important for normal expression of *osm-5*.

OSM-5 acts as a component of the IFT raft

Characterization of several ciliary mutants with a similar phenotype as seen in *osm-5* worms has shown that the responsible proteins are components of the IFT process. The ciliary localization of OSM-5, along with the loss of cilia in mutants raises the possibility that OSM-5 is another IFT component. To address this possibility, we conducted time-lapse fluorescence imaging on the amphids and phasmids of the OSM-5::GFP transgenic worms using an approach similar to that reported for the analysis of OSM-1, OSM-3 and OSM-6 (Orozco et al., 1999; Signor et al., 1999a). In sequential frames, fluorescent particles can be detected migrating in both anterograde and retrograde directions within the cilium (Fig. 8). Thus, the data in this manuscript support a role for OSM-5 in a ciliogenic pathway most likely as a component of the IFT system.

DISCUSSION

The *Tg737* gene was originally identified because of its association with the *Oak Ridge Polycystic Kidney* mouse mutation. Although the role for the *Tg737* protein (polaris) is still uncertain, the pathology in several tissues is associated with defects in the formation or maintenance of cilia. In this report, we further the analysis of *Tg737* function by identifying and characterizing its homolog in *C. elegans*, the gene *Y41g9a.1*. The protein product of *Y41g9a.1* shares greater than 45% identity over the entire length of the mouse and human polaris sequences. We show that mutations in *Y41g9a.1* are responsible for the cilia defects in the *osm-5* mutant worms by characterizing three independent *osm-5* alleles and by rescuing these defects in *osm-5(p813)* animals with the wild-type *Y41g9a.1* gene. In agreement with a ciliogenic role, *osm-5* expression appears exclusive to ciliated sensory neurons in the worm, beginning at approximately the twofold stage of embryogenesis, coinciding with the start of cilia extension. As reported for several other genes involved in ciliogenesis in *C. elegans*, *osm-5* expression is regulated by the DAF-19 transcription factor in an X-box-dependent manner (Swoboda et al., 2000). Furthermore, the OSM-5 protein was found to concentrate at the distal end of the dendrites in the transition zone and within cilia. Finally, using an OSM-5::GFP fusion protein we are able to demonstrate that OSM-5 probably functions as a component of the IFT system, as revealed by migration of fluorescent GFP particles in the cilia of the amphids and phasmids. Overall, our analysis of the *Tg737* homolog in the worm indicates that it is a highly conserved gene present in organisms that range from the flagellated eukaryote *T. brucei* to humans, where it probably plays a common role in cilia or flagella formation.

It has previously been demonstrated that *osm-5* mutants exhibit severe truncation of all cilia on the sensory neurons (Perkins et al., 1986). In contrast to these cilia defects, mutations in *osm-5* have relatively little effect on other aspects of the morphology of the two sensory neurons (AFD and ASE) analyzed here. Specifically, cell bodies were present and positioned correctly and dendritic and axonal trajectories were grossly normal. The specificity of *osm-5* mutations on ciliary formation is further supported by the fact that another sensory specialization on the distal end of dendrites, namely the finger-like microvilli of AFD, was unaffected. However, we did observe extraneous short processes in addition to normal axons and dendrites. These structures have been reported in mutations in a diverse set of genes, including other cilium structure genes, indicating that these low penetrance abnormalities are not *osm-5* specific (Coburn and Bargmann, 1996; Coburn et al., 1998; Hobert et al., 1997; Peckol et al., 1999; Wittenburg et al.,

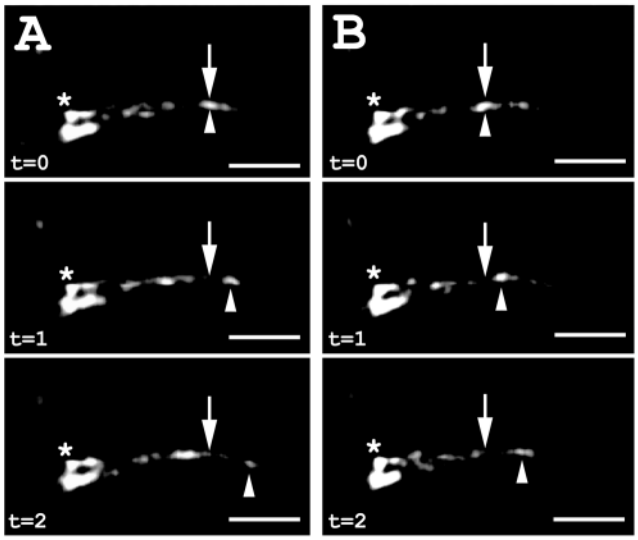

Fig. 8. Movement of OSM-5::GFP in cilia of one pair of phasmid neurons. Two sequences from the same worm are shown, each composed of three sequential frames. Anterior is towards the left. The asterisk is located at the transition zones of both cilia. The arrow indicates the initial position of the fluorescent particle at time 0 in all frames. The arrowhead indicates the location of the fluorescent particle in each frame. In both sequences (A) and (B), the particle indicated moves in the anterograde direction. Scale bars: 2.5 μm.

2000). The specificity of the phenotype in *osm-5* mutants suggests that *osm-5* functions late in the differentiation of the sensory neurons where it is required for normal formation or maintenance of cilia.

One of the advantages of the completed *C. elegans* genome is that it allows a search of the entire genome for promoter elements that might be important for the common regulation of a group of genes that function in the same process. For example, several genes involved in cilia formation in *C. elegans* appear to be regulated in DAF-19- and X-box-dependent manners (Swoboda et al., 2000). Furthermore, the partial genome sequences available from the closely related nematode *C. briggsae* allows the comparison of these upstream sequences between the two species to identify potential promoter elements, which are more likely to be conserved than intergenic regions. Using this approach, we identified two conserved domains in the *osm-5* promoter. One of these elements was a near consensus X-box. This promoter element has previously been identified in a subgroup of ciliogenic genes expressed in all ciliated sensory neurons of the worm, including *che-2*, *daf-19*, *osm-1*, *osm-6* and now in *osm-5* (Swoboda et al., 2000). These genes have long been grouped together on the basis of the severe cilia defects observed upon their mutation (Perkins et al., 1986). Mutations in *che-2*, *osm-1*, *osm-5* and *osm-6* result in loss of the middle and distal segments of cilia, while loss of functional DAF-19 also results in loss of the transition zone located at the base of cilia. As seen in promoters of several other ciliogenic genes, the X-box in the *osm-5* promoter appears crucial for its regulation. The reduced expression in the *daf-19* mutant background was detected using three separate assays, including an *osm-5*::GFP transcriptional construct, by northern blot analysis, and by immunofluorescence. Overall, these data fit a model in which DAF-19 functions as a key transcriptional regulator of the ciliogenic pathway in the worm. Whether a similar regulatory mechanism exists for *Tg737* and other ciliogenic genes in higher eukaryotes has yet to be determined; however, it is interesting that a near consensus X-box sequence is also located upstream of the *Tg737* gene in the mouse (B. K. Y., unpublished).

Information regarding the functional domains of a protein can often be obtained through characterization of multiple alleles. In the case of *osm-5*, there are six independent alleles (Starich et al., 1995), three of which we characterize here. The reference allele *p813* contains a nonsense mutation that predicts a truncated protein lacking its C-terminal half. As this truncated protein still concentrates at the distal tips of dendrites at nearly wild-type levels, it would suggest that the N-terminal region of OSM-5 is sufficient for its localization but not for cilia formation. In the second allele analyzed, *mn397*, we detected a missense mutation that results in the substitution of Glu for Gly in the eighth position of the second TPR motif. This position is an invariantly conserved Gly in all polaris (*Tg737*) homologs identified to date. Furthermore, it is one of the most crucial residues within the TPR motif in general, where the eighth residue is normally a small nonpolar residue such as Gly, Ala or Ser (Das et al., 1998). Similar to what we find in the *mn397* allele, functional perturbing mutations in the eighth residue of TPRs in yeast protein cdc23 and in the human protein p67 phox have also been identified (de Boer et al., 1994; Sikorski et al., 1993). The effect of a mutation in the eighth position of a TPR on these proteins can be predicted by the crystal structure determined for the three tandem TPR motifs in protein phosphatase 5 (PP5) (Das et al., 1998). The structure indicates that residue 8 is one of the closest points of contact between the two α-helices that characterize a TPR motif. Thus, the substitution of a polar Glu for Gly at this position would likely interfere with the hydrophobic interactions required for proper folding of the TPR motif. One possibility is that the mutation causes general misfolding of OSM-5; however, the fact that the mutated protein still localizes correctly to the distal tip of the dendrite suggests that this may not be the case. Alternatively, this mutation could abolish the hydrophobic cleft predicted from the crystal structure that is thought to be required for the interaction of PP5 with its substrates. In PP5, the cleft is generated by the three tandem TPRs as seen in the N-terminal region of OSM-5, thus the mutation in *mn397* could specifically prevent the interaction of OSM-5 with another protein(s) involved in ciliogenesis.

The final allele characterized was *sa130*. This mutation occurs in the 5′ splice donor site of the third *osm-5* exon. Of the three *osm-5* mutations characterized, this allele is the most likely candidate for a null. However, OSM-5 protein was still detected by immunofluorescence at the transition zone using two different monoclonal antibodies raised against amino acids 238 to 660, although at markedly reduced levels. Although preincubation of the antisera with purified OSM-5::GST fusion protein can block the immunolocalization in wild-type worms, we cannot unequivocally exclude the possibility that there is another protein specific to cilia that shares a common epitope with OSM-5 and thus would still be present in the *sa130* mutants. This protein would also be regulated by DAF-19, as both antibodies show reduced expression in the *daf-19* mutant background. Alternatively, a more feasible explanation for the continued low level of OSM-5 protein might be the use of nonconsensus or cryptic splice donor sites, such as the AU present in the *sa130* allele. This has previously been reported for similar splice donor mutations in other *C. elegans* genes where cryptic splice sites are able to excise the Tc1 insertion (Rushforth and Anderson, 1996). In these mutations, the resulting mRNAs contain a number of splicing variations, some of which do not alter the reading frame, but contain small functional perturbing insertions or deletions, owing to the use of these cryptic donor sites.

An observation that is becoming clear from the characterization of genes involved in cilia or flagella formation is that they are highly conserved across a broad range of organisms (Cole et al., 1998; Collet et al., 1998; Signor et al., 1999a). Many of these genes are involved in intraflagellar transport, a process required for cilia formation and maintenance. According to this model, ciliogenic proteins concentrate in transition zones or basal bodies near the base of cilia where they pre-assemble into protein rafts (Cole et al., 1998). These rafts are transported up and down the cilia axoneme by microtubule based motor proteins such as kinesins and dyneins. We show that the OSM-5 protein, as previously reported for the proteins OSM-1 and OSM-6, exhibits the localization pattern characteristic of an IFT protein. Furthermore, mutations in *osm-5* cause cilia structure defects that are markedly similar to that seen in *osm-1* and *osm-6* mutants as determined at the level of electron

microscopy (Perkins et al., 1986). Finally, using the OSM-5::GFP translational fusion we demonstrate both anterograde and retrograde movement of the fluorescent particles within the cilia with velocities similar to that reported for other IFT particles by Signor et al. (Signor et al., 1999a). From these data, we predict that OSM-5 is another core component of the IFT system. A role for OSM-5 in IFT as cargo or as part of the raft itself is yet to be determined; however, the fact that OSM-5 contains ten copies of the TPR, a motif known to mediate protein complex formation, suggests that it could serve as a scaffold upon which the other IFT raft proteins assemble.

In the mouse, mutations in *Tg737* result in a complex pathology involving polycystic kidney disease, random left-right axis specification, hydrocephalus, and skeletal patterning abnormalities (Moyer et al., 1994; Murcia et al., 2000; Taulman et al., 2001). Similar to what we see in *osm-5* mutants, loss of *Tg737* in mice appears to be associated with ciliary abnormalities (Murcia et al., 2000; Pazour et al., 2000; Taulman et al., 2001). The common ciliary defects along with the high sequence conservation of this protein across a diverse group of ciliated and flagellated eukaryotes suggest that polaris (*Tg737*) and its homologs may play similar roles in all these organisms. Thus, further molecular characterization of OSM-5 and the proteins with which it interacts in *C. elegans* will probably yield important insight into how disruption of this protein can lead to the severe developmental abnormalities and disease states seen in *Tg737* mutant mice. This is particularly relevant with regards to polycystic kidney disease (PKD). Two additional *C. elegans* homologs (*lov-1* and *pkd-2*) of genes involved in mammalian PKD (*pkd-1* and *pkd-2*) have been identified (Barr and Sternberg, 1999). Interestingly, *osm-5*, *lov-1* and *pkd-2* are expressed in ciliated sensory neurons; however, in contrast to *osm-5*, *lov-1* appears to be expressed only in males. While cilia appear normal in *lov-1* mutants, males exhibit difficulties in locating the hermaphrodite vulva, suggesting there is a defect in sensory perception similar to *osm-5* mutants (Barr and Sternberg, 1999). The fact that all three genes are expressed in a common subset of ciliated sensory neurons and mutations in the homologs of these genes in mammals result in cystic kidney pathology suggests that they may be involved in a similar signaling pathway. Thus, exploring potential molecular and genetic interactions of these proteins using *C. elegans* as a model system will probably give crucial insight into the molecular pathology of this common human disorder.

We thank the following people for technical assistance, helpful discussions, unpublished information, *C. elegans* strains, cosmid and cDNA clones, and GFP vectors: K. Bubb, A. Coulson, A. Fire, R. Herman and especially members of our laboratories. We also thank D. Miller for critical reading of the manuscript; M. Accavitti and the UAB Hybridoma Core for assistance with antibody production (supported by grant 5P60-AR-20614); and A. Tousson and S. Williams of the UAB High Resolution Imaging Facility for assistance in image generation. We thank the *C. elegans* Genome Sequencing Consortium for providing genome sequence information and the Caenorhabditis Genetics Center, which is funded by the National Institutes of Health, for providing some of the *C. elegans* strains used in this study. This work was supported in part by NIH R01 to B. K. Y. (R01 DK55007) and by a Public Health Service Grant to J. H. T. (R01 GM48700). P. S. was supported by postdoctoral fellowships from the Erwin Schrödinger Foundation (Vienna, Austria) and from the Human Frontier Science Promotion Organization (Strasbourg, France).

REFERENCES

Agard, D. A., Hiraoka, Y., Shaw, P. and Sedat, J. W. (1989). Fluorescence microscopy in three dimensions. *Methods Cell Biol.* **30**, 353-377.

Apfeld, J. and Kenyon, C. (1999). Regulation of lifespan by sensory perception in Caenorhabditis elegans. *Nature* **402**, 804-809.

Bargmann, C. I. and Horvitz, H. R. (1991). Chemosensory neurons with overlapping functions direct chemotaxis to multiple chemicals in C. elegans. *Neuron* **7**, 729-742.

Barr, M. M. and Sternberg, P. W. (1999). A polycystic kidney-disease gene homologue required for male mating behaviour in C. elegans. *Nature* **401**, 386-389.

Blatch, G. L. and Lassle, M. (1999). The tetratricopeptide repeat: a structural motif mediating protein-protein interactions. *BioEssays* **21**, 932-939.

Brenner, S. (1974). The genetics of Caenorhabditis elegans. *Genetics* **77**, 71-94.

***C. elegans* Sequencing Consortium** (1998). Genome sequence of the nematode C. elegans: a platform for investigating biology. *Science* **282**, 2012-2018.

Coburn, C. M. and Bargmann, C. I. (1996). A putative cyclic nucleotide-gated channel is required for sensory development and function in C. elegans. *Neuron* **17**, 695-706.

Coburn, C. M., Mori, I., Ohshima, Y. and Bargmann, C. I. (1998). A cyclic nucleotide-gated channel inhibits sensory axon outgrowth in larval and adult Caenorhabditis elegans: a distinct pathway for maintenance of sensory axon structure. *Development* **125**, 249-258.

Cole, D. G., Diener, D. R., Himelblau, A. L., Beech, P. L., Fuster, J. C. and Rosenbaum, J. L. (1998). Chlamydomonas kinesin-II-dependent intraflagellar transport (IFT): IFT particles contain proteins required for ciliary assembly in Caenorhabditis elegans sensory neurons. *J. Cell Biol.* **141**, 993-1008.

Collet, J., Spike, C. A., Lundquist, E. A., Shaw, J. E. and Herman, R. K. (1998). Analysis of osm-6, a gene that affects sensory cilium structure and sensory neuron function in Caenorhabditis elegans. *Genetics* **148**, 187-200.

Culotti, J. G. and Russell, R. L. (1978). Osmotic avoidance defective mutants of the nematode Caenorhabditis elegans. *Genetics* **90**, 243-256.

Das, A. K., Cohen, P. W. and Barford, D. (1998). The structure of the tetratricopeptide repeats of protein phosphatase 5: implications for TPR-mediated protein-protein interactions. *EMBO J.* **17**, 1192-1199.

de Boer, M., Hilarius-Stokman, P. M., Hossle, J. P., Verhoeven, A. J., Graf, N., Kenney, R. T., Seger, R. and Roos, D. (1994). Autosomal recessive chronic granulomatous disease with absence of the 67-kD cytosolic NADPH oxidase component: identification of mutation and detection of carriers. *Blood* **83**, 531-536.

Dusenbery, D. B., Sheridan, R. E. and Russell, R. L. (1975). Chemotaxis-defective mutants of the nematode Caenorhabditis elegans. *Genetics* **80**, 297-309.

Dutcher, S., K. (1995). Flagellar assembly in two hundred easy-to-follow steps. *Trends Genet.* **11**, 398-404.

Dwyer, N. D., Troemel, E. R., Sengupta, P. and Bargmann, C. I. (1998). Odorant receptor localization to olfactory cilia is mediated by ODR-4, a novel membrane-associated protein. *Cell* **93**, 455-466.

Frangioni, J. V. and Neel, B. G. (1993). Solubilization and purification of enzymatically active glutathione S-transferase (pGEX) fusion proteins. *Anal. Biochem.* **210**, 179-87.

Fujiwara, M., Ishihara, T. and Katsura, I. (1999). A novel WD40 protein, CHE-2, acts cell-autonomously in the formation of C. elegans sensory cilia. *Development* **126**, 4839-4848.

Hall, D. H. and Russell, R. L. (1991). The posterior nervous system of the nematode Caenorhabditis elegans: serial reconstruction of identified neurons and complete pattern of synaptic interactions. *J. Neurosci.* **11**, 1-22.

Hobert, O., Mori, I., Yamashita, Y., Honda, H., Ohshima, Y., Liu, Y. and Ruvkun, G. (1997). Regulation of interneuron function in the C. elegans thermoregulatory pathway by the ttx-3 LIM homeobox gene. *Neuron* **19**, 345-357.

Krause, M., Wild, M., Rosenzweig, B. and Hirsh, D. (1989). Wild-type and mutant actin genes in Caenorhabditis elegans. *J. Mol. Biol.* **208**, 381-392.

Marszalek, J. R., Ruiz-Lozano, P., Roberts, E., Chien, K. R. and Goldstein, L. S. (1999). Situs inversus and embryonic ciliary morphogenesis defects in

mouse mutants lacking the KIF3A subunit of kinesin-II. *Proc.Natl. Acad. Sci. USA* **96**, 5043-5048.

Mello, C. C., Kramer, J. M., Stinchcomb, D. and Ambros, V. (1991). Efficient gene transfer in C.elegans: extrachromosomal maintenance and integration of transforming sequences. *EMBO J.* **10**, 3959-3970.

Miller, D. M. and Shakes, D. C. (1995). Immunofluorescence Microscopy. In Caenorhabditis elegans: *Modern Biological Analysis of an Organism* (ed. H. F. Epstein and D. C. Shakes), pp. 365-394. San Diego, CA: Academic Press.

Mori, I. and Ohshima, Y. (1997). Molecular neurogenetics of chemotaxis and thermotaxis in the nematode Caenorhabditis elegans. *BioEssays* **19**, 1055-1064.

Moyer, J. H., Lee-Tischler, M. J., Kwon, H. Y., Schrick, J. J., Avner, E. D., Sweeney, W. E., Godfrey, V. L., Cacheiro, N. L., Wilkinson, J. E. and Woychik, R. P. (1994). Candidate gene associated with a mutation causing recessive polycystic kidney disease in mice. *Science* **264**, 1329-1333.

Murcia, N. S., Richards, W. G., Yoder, B. K., Mucenski, M. L., Dunlap, J. R. and Woychik, R. P. (2000). The Oak Ridge Polycystic Kidney (orpk) disease gene is required for left-right axis determination. *Development* **127**, 2347-2355.

Nonaka, S., Tanaka, Y., Okada, Y., Takeda, S., Harada, A., Kanai, Y., Kido, M. and Hirokawa, N. (1998). Randomization of left-right asymmetry due to loss of nodal cilia generating leftward flow of extraembryonic fluid in mice lacking KIF3B motor protein. *Cell* **95**, 829-37.

Okada, Y., Nonaka, S., Tanaka, Y., Saijoh, Y., Hamada, H. and Hirokawa, N. (1999). Abnormal nodal flow precedes situs inversus in iv and inv mice. *Mol. Cell* **4**, 459-468.

Orozco, J. T., Wedaman, K. P., Signor, D., Brown, H., Rose, L. and Scholey, J. M. (1999). Movement of motor and cargo along cilia. *Nature* **398**, 674.

Pazour, G. J., Dickert, B. L., Vucica, Y., Seeley, E. S., Rosenbaum, J. L., Witman, G. B. and Cole, D. G. (2000). Chlamydomonas IFT88 and its mouse homologue, polycystic kidney disease gene Tg737, are required for assembly of cilia and flagella. *J. Cell Biol.* **151**, 709-718.

Peckol, E. L., Zallen, J. A., Yarrow, J. C. and Bargmann, C. I. (1999). Sensory activity affects sensory axon development in C. elegans. *Development* **126**, 1891-1902.

Perkins, L. A., Hedgecock, E. M., Thomson, J. N. and Culotti, J. G. (1986). Mutant sensory cilia in the nematode Caenorhabditis elegans. *Dev. Biol.***117**, 456-487.

Piperno, G. and Mead, K. (1997). Transplant of a novel complex in the cytoplasmic matrix of *Chlamydomonas* flagella. *Proc. Natl. Acad. Sci. USA* **94**, 4457-4462.

Rushforth, A. M. and Anderson, P. (1996). Splicing removes the Caenorhabditis elegans transposon Tc1 from most mutant pre-mRNAs. *Mol. Cell. Biol.* **16**, 422-429.

Sambrook, J., Fritsch, E. F. and Maniatis, T. (1989). *Molecular Cloning: A Laboratory Manual*. Cold Spring Harbor, NY: Cold Spring Harbor Laboratory Press.

Scalettar, B. A., Swedlow, J. R., Sedat, J. W. and Agard, D. A. (1996). Dispersion, aberration and deconvolution in multi-wavelength fluorescence images. *J. Microsc.* **182**, 50-60.

Schrick, J. J., Onuchic, L. F., Reeders, S. T., Korenberg, J., Chen, X. N., Moyer, J. H., Wilkinson, J. E. and Woychik, R. P. (1995). Characterization of the human homologue of the mouse Tg737 candidate polycystic kidney disease gene. *Hum. Mol. Genet.* **4**, 559-567.

Shakir, M. A., Fukushige, T., Yasuda, H., Miwa, J. and Siddiqui, S. S. (1993). C. elegans osm-3 gene mediating osmotic avoidance behaviour encodes a kinesin-like protein. *NeuroReport* **4**, 891-894.

Signor, D., Wedaman, K. P., Orozco, J. T., Dwyer, N. D., Bargmann, C. I., Rose, L. S. and Scholey, J. M. (1999a). Role of a class DHC1b dynein in retrograde transport of IFT motors and IFT raft particles along cilia, but not dendrites, in chemosensory neurons of living Caenorhabditis elegans. *J. Cell Biol.* **147**, 519-530.

Signor, D., Wedaman, K. P., Rose, L. S. and Scholey, J. M. (1999b). Two heteromeric kinesin complexes in chemosensory neurons and sensory cilia of Caenorhabditis elegans. *Mol. Biol. Cell* **10**, 345-360.

Sikorski, R. S., Michaud, W. A. and Hieter, P. (1993). p62cdc23 of Saccharomyces cerevisiae: a nuclear tetratricopeptide repeat protein with two mutable domains. *Mol. Cell. Biol.* **13**, 1212-21.

Starich, T. A., Herman, R. K., Kari, C. K., Yeh, W. H., Schackwitz, W. S., Schuyler, M. W., Collet, J., Thomas, J. H. and Riddle, D. L. (1995). Mutations affecting the chemosensory neurons of Caenorhabditis elegans. *Genetics* **139**, 171-188.

Swoboda, P., Adler, H. T. and Thomas, J. H. (2000). The RFX-type transcription factor DAF-19 regulates sensory neuron cilium formation in C. elegans. *Mol. Cell* **5**, 411-421.

Taulman, P. D., Haycraft, C. J., Balkovetz, D. F. and Yoder, B. K. (2001). Polaris, a protein involved in left-right axis patterning localizes to basal bodies and cilia. *Mol. Biol. Cell* (in press).

Vowels, J. J. and Thomas, J. H. (1992). Genetic analysis of chemosensory control of dauer formation in Caenorhabditis elegans. *Genetics* **130**, 105-123.

Ward, S., Thomson, N., White, J. G. and Brenner, S. (1975). Electron microscopical reconstruction of the anterior sensory anatomy of the nematode Caenorhabditis elegans. *J. Comp. Neurol.* **160**, 313-337.

Ware R., W., Clark, D., Crossland, K. and Russell, R., L. (1975). The nerve ring of the nematode Caenorhabditis elegans: sensory input and motor out. *J. Comp. Neurol.* **162**, 71-110.

White, J. G., Southgate, E., Thomson, J. N. and Brenner, S. (1986). The structure of the nervous system of the nematode Caenorhabditis elegans. *Philos. Trans. R. Soc. London Ser. B Biol. Sci.* **314**, 1-340.

Wicks, S., de Vries, C., van Luenen, H. and Plasterk, R. (2000). CHE-3, a cytosolic dynein heavy chain, is required for sensory cilia structure and function in caenorhabditis elegans. *Dev. Biol.* **221**, 295-307.

Wittenburg, N., Eimer, S., Lakowski, B., Rohrig, S., Rudolph, C. and Baumeister, R. (2000). Presenilin is required for proper morphology and function of neurons in C. elegans. *Nature* **406**, 306-309.

Yoder, B. K., Richards, W. G., Sommardahl, C., Sweeney, W. E., Michaud, E. J., Wilkinson, J. E., Avner, E. D. and Woychik, R. P. (1997). Differential rescue of the renal and hepatic disease in an autosomal recessive polycystic kidney disease mouse mutant. A new model to study the liver lesion. *Am. J. Pathol.* **150**, 2231-2241.

Yu, S., Avery, L., Baude, E. and Garbers, D. L. (1997). Guanylyl cyclase expression in specific sensory neurons: a new family of chemosensory receptors. *Proc. Natl. Acad. Sci. USA* **94**, 3384-3387.